Autonomous Precise Assembly of Segmented Mirror Tiles for a Space Telescope

Máximo A. Roa, Korbinian Nottensteiner, Ismael Rodríguez, Timo Bachmann, Jean-Pascal Lutze
German Aerospace Center (DLR)
Institute of Robotics and Mechatronics
Münchner Str. 20, 82234 Weßling, Germany
maximo.roa@dlr.de

Pierre Letier
Space Application Services
Leuvensesteenweg 325
1932 Sint-Stevens-Woluwe, Belgium
pierre.letier@spaceapplications.com

Antoine Ummel, Julien Rouvinet, Florent Cosandier, David Nguyen, Virginien Schaffter
CSEM
Rue Jaquet-Droz 1
2002 Neuchâtel, Switzerland
antoine.ummel@csem.ch

Souriya Trinh, Vincent Bissonnette Thierry Germa
Magellium
1 rue Ariane
31520 Ramonville Saint-Agne Cedex, France
thierry.germa@magellium.fr

***Abstract*— Future space applications require the assembly of large structures in orbit. This can only be achieved by using autonomous robotic systems able to handle repetitive tasks with heavy and large parts in such challenging environment. This paper provides an overview of a system designed to perform autonomous assembly of segmented mirror tiles, as a proof of feasibility for assembling large structures in space using robotic technologies. We describe the hardware components of the system, and present the software layer, including assembly planning, and skill engine. An experimental evaluation of the assembly process is carried out, thus showing the performance achieved with the system.**

TABLE OF CONTENTS

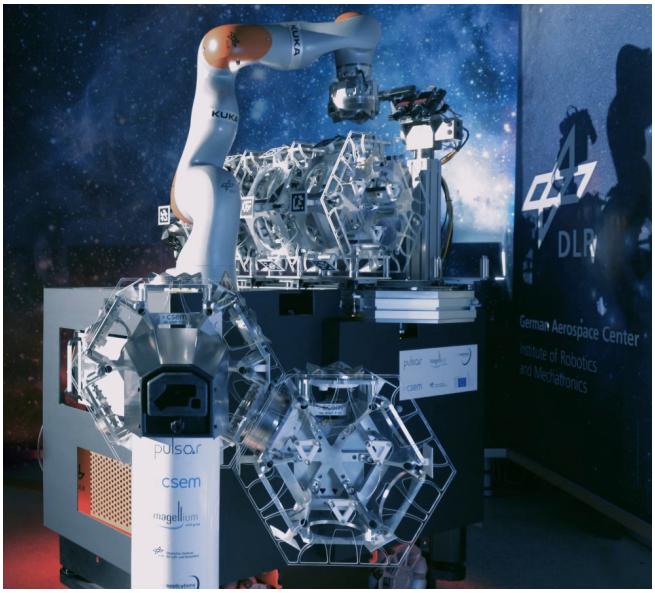

Figure 1. Robotic system for autonomous assembly of the primary mirror of a telescope using segmented mirror tiles that are connected via standard interconnects.

1. INTRODUCTION

The future of space exploration requires large space structures, including for instance space telescopes, solar arrays for large space-based power plants or data centers, or space stations that replace the ISS. All of these structures have in common that they are too large to be deployed on a single piece. Recently, the James Webb Space Telescope (JWST) used an ingenious folding mechanism to be able to fit its 6.5 m primary mirror inside the 5.4 m diameter cargo area of its launcher, an Ariane 5 rocket [1]. For deploying larger structures, parts and subcomponents should be launched to space and assembled directly in orbit using autonomous robotic systems, without requiring intervention of astronauts or ground control.

Assembling a large space structure implies putting together modular components in an ordered fashion, dictated by a high-level master plan that indicates the relative positioning of each part. In space applications, common robotic systems have a small degree of autonomy for task execution. Operations usually rely on remote commands, which require an appropriate feedback channel for the operator, typically affected by substantial time delays. The concept of shared autonomy increases the dexterity of such robotic systems and reduces the effort for the operators in complex tasks. Nevertheless, remote operation approaches have limited use when it comes to the assembly of complex structures because of the fine granularity of assembly tasks, as the synchronization of operator commands and manipulator actions would consume

979-8-3503-0462-6/24/$31.00 ©2024 IEEE

substantial amounts of time. Therefore, a robotic assembly system should be capable of autonomously performing a sequence of operations or even the complete assembly task.

One of the promising applications for space-based assembly is the construction of a large space telescope. Different proposals on how to achieve such goal have been made [2]. The various technological building blocks required for such in-space assembly have diverse levels of maturity. Highly mature technologies include launch vehicles, and mirror segment fabrication. Medium maturity include segmented mirror wavefront and jitter control, and robotic hardware (arms). However, the aspects with lower level of maturity are related to the planning, control and execution of in-space robotic autonomous assembly [3].

Different research projects investigate new applications for in-space assembly, including for instance modular reconfigurable satellites, as in the project MOSAR (MOdular Spacecraft Assembly and Reconfiguration) [4], and large structures such as telescopes, as in the project PULSAR (Prototype of an Ultra Large Structure Assembly Robot [5]). The latter project, funded by the European Commission H2020 Strategic Research Cluster (SRC), considered specifically the development and demonstration of technologies required for assembling a segmented mirror for a telescope using an autonomous robotic system (Fig. 1). PULSAR was organized in three demonstration tracks to address different aspects of the problem:

1. dPAMT, demonstrator of Precise Assembly of Mirror Tiles: addressed the challenge of assembling a mirror composed by multiple hexagonal segmented mirror tiles.
2. dLSAFFE, demonstrator of Large Structure Assembly in Free Floating Environment: addressed the challenge of assembling a large structure in a free-floating environment, in this case, underwater.
3. dISAS, demonstrator of In-Space Assembly in Simulation, addressed the challenge of simulating in the most realistic conditions possible the deployment of a large structure while ensuring stability and safety of the spacecraft.

Our work presents the results obtained with dPAMT, a physical demonstrator used to verify the feasibility of performing the robotic assembly of a telescope mirror using an autonomous robot. The primary mirror of the telescope is composed by multiple segmented mirror tiles (SMTs). The connectivity between the tiles is guaranteed using standard interconnects, which provide mechanical, power, and data connetions. To create the sequence of assembly steps, an assembly planning system verifies at a semantic level the different constraints that the structure must fulfill, including data and power connectivity, and overall mechanical stability of the structure. The planning system generates an assembly sequence, which is mapped to robot skills and executed using a skill engine. The skills are parameterized in reusable actions that the robotic system can perform to execute the assembly. In our case, we use a torque-based robot, which uses compliant control to perform the assembly of the overall structure. For performing the verification of the assembly, each SMT is endowed with AprilTag markers and Vicon spheres, for intrinsic and extrinsic verification of the assembly outcome.

The paper is organized as follows. After a brief overview of related work in space-based assembly in Section 2, the system overview is presented in Section 3. Section 4 shows the experimental results obtained with our setup, and conclusions are presented in Section 5.

2. SPACE-BASED ASSEMBLY

Autonomous operations in space are still very challenging, and only a limited number of demonstrations on orbit have been performed. The first successful demonstration of an unmanned spacecraft to conduct autonomous rendezvous and docking operations was done by NASDA (now JAXA) in 1999 on ETS-VII [6]. It was the first satellite equipped with a robotic arm that allowed ESA to conduct the VIABLE experiment, demonstrating computer vision support for autonomous robot control [7].

Several robotic arms are now installed on board the ISS, including Canadarm, Dextre, Kibo and ERA, but for now they are used for astronaut support, directly controlled in space, or in operations remotely controlled from ground [8]. Autonomous robotic assembly of space systems has been demonstrated on ground for planar truss and beam structures, but their test in orbit and with more complex structures still remains a challenge. Among the missions under development, NASA's OSAM-1 (formerly Restore-L) and DARPA's MRV (formerly RSGS) are expected to demonstrate in the near future the autonomy and dexterity required for on-orbit assembly. An overview of current technologies for in-space assembly is provided in [9], [3], [10].

For space telescopes, current monolithic designs have reached the limits of the available cargo areas in launch vehicles. To push forward the size of space telescopes, current engineering approaches aim for a deployable structure that can be packed inside the current cargo areas, as in the case of the JWST, or a modular design that can be deployed and assembled in space. For the latter, a risk vs. cost tradeoff must be done between first time assembly and reassembly, i.e. either the telescope components are directly launched and assembled for the first time in space, or the telescope is assembled and tested on ground, then taken apart and launched to be reassembled in space. Other requirements for the new generation of space telescopes include serviceability, to allow replacement and upgrading of instruments and subsystems as required, refueling and repairing on demand, and expandability, i.e. incremental enlargement of the aperture over time when the design allows it. The key question for this new approach is: When does in-space assembly of telescopes represent an advantage (lower risk, lower price) over building them on Earth and sending them as a single piece? Tradeoffs for large telescope designs, and effects of different design decisions on the missions, are discussed in detail in [11], [12].

An overview of technologies for in-space assembly of space telescopes is provided in [2]. Different approaches have been proposed for this purpose, mainly using three techniques:

- Deployable structures: following the idea of JWST for launching a single structure deployed once it has reached its intended location, several proposals have been made, including ATLAST (Advanced Technology Large Aperture Space Telescope) [13] or LUVOIR (Large Ultraviolet Optical Infrared Telescope) [14].
- Free-flying satellites: alternative ideas to create a telescope using individual mirror components mounted on different small satellites have been also explored, e.g. GOAT (Giant Orbiting Astronomical Telescope) [15].
- Assembly using robot manipulators: different robotic systems have been proposed to perform on-orbit assembly of a telescope, including single and dual arm manipulators rigidly attached to a spacecraft, wheeled robots that move on rails on top of a satellite or on top of the structure being assembled, or robots using a walking strategy that allows the robot to

move on top of the spacecraft, attaching and detaching from the satellite as required. Proposals in this direction include AAST (Autonomously Assembled Space Telescope) [16], EST (Evolvable Space Telescope) [17] or RAMST (Robotically Assembled Modular Space Telescope) [18].

3. System Overview

This section provides an overview of the implemented system, both in terms of hardware with the description of the standard interconnects, the SMTs and the robotic system, and software, with the description of the assembly planning system, the skill engine - including compliant control strategies-, and the visual perception pipeline.

Requirements

The overall goal of the dPAMT setup was to demonstrate the precise assembly of mirror tiles using an autonomous robotic system. The demonstration was planned to be carried out on ground, which adds multiple constraints and requirements on the setup. Consequently, capabilities to be demonstrated and related requirements on the system are as follows:

- A mobile base is required to relocate the robot manipulator, as the size of the assembled mirror exceeds the workspace of the robotic arm
- A visual perception system is required to monitor the assembly progress
- A force-sensitive robot is required to compensate for remaining geometric uncertainties during the assembly process
- The mass properties and dimensions of the mirror tiles should fulfill the constraints of maximum payload in the robot manipulator
- A standard interconnect is required to facilitate the manipulation and assembly of the mirror tiles. The interconnect should provide not only mechanical, but also electrical and data connectivity between the mirror tiles.
- The mirror tiles should have a positioning system to realign the mirror surfaces after the assembly process is concluded

Segmented mirror tiles

For the selected demonstration scenario, a total of 6 SMTs are developed. Two of these tiles are *active*: they accommodate a mirror positioning mechanism to demonstrate the capability to correct inaccuracies generated by manufacturing tolerances, gravitational effects in the test setup, and the autonomous robotic assembly process. The four other tiles are *passive*. The configuration of the various tiles used to conform the primary mirror is displayed in Fig 2.

Each SMT is equipped with standard HOTDOCK interfaces, allowing it to be manipulated by the robotic arm and interfaced with one or more other tiles. The mechanics of the SMTs and HOTDOCKs are designed to withstand the loads expected in the demonstration scenario and to ensure structural stability and integrity. The possible load transfer of a single HOTDOCK is 3000 N in traction and 300 Nm in bending moment [19]. The SMTs are also equipped with fiducial markers (AprilTags) so that they can be identified and located by the robotic vision system. In addition, reflector spheres are mounted on the fixed parts of all tiles and on the mobile stage of the active tiles to enable more accurate measurements of the overall positions of the mirror structure using a VICON system as ground truth measurement system. For the SMTs, the telescope mirrors are replaced by a transparent lightweight dummy. These features can be seen on Fig. 3, which illustrates a passive and an active tile.

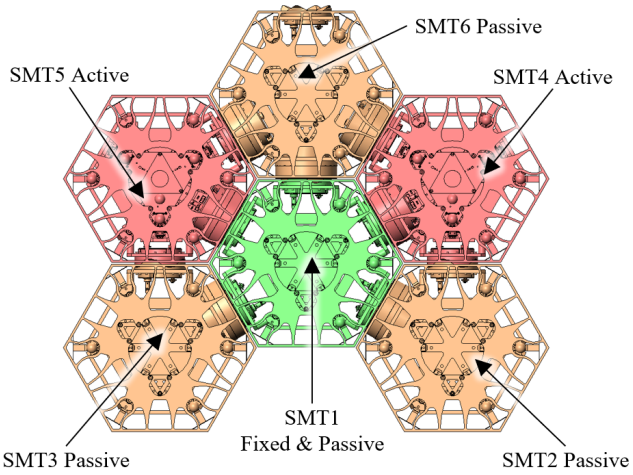

Figure 2. Configuration of mirror tiles in the full mirror.

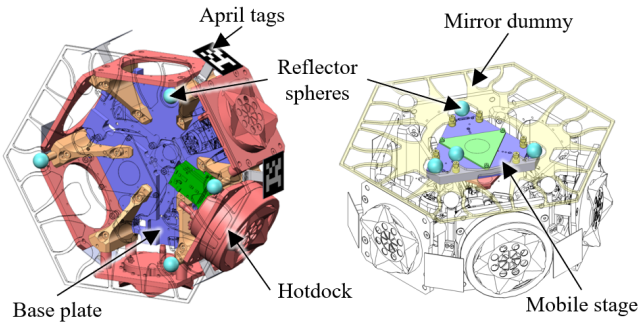

Figure 3. Passive (left) and active (right) segmented mirror tile.

Furthermore, the mass properties of the SMTs are listed in Table 1, which are needed to set the load data in the robot control during manipulation of the tiles.

The SMT positioning mechanism kinematics is shown in Fig. 4. The three pods are each composed of a *linear stage*, mounted radially, on which single axis flexure pivots are mounted. The pivots are linked to a 3-rotation axes gimbal, and the mobile mirror stage is connected to the three gimbals. This structure has no internal degrees of freedom and is isostatic, which is an asset towards high precision performance. The assembly of flexure pivots and gimbals is referred to as the *flexible transmission stage* of the mechanism.

To control the position of the mechanism, a sensor and an actuator are implemented directly on the linear stage of each pod. This implementation greatly simplifies the hardware

Table 1. Mass properties of the manipulated SMTs.

SMT	2	3	4	5	6	
Mass	7.53	7.53	9.97	9.93	10.54	kg
COM_x	27.3	-27.3	29.0	-28.7	5.8	mm
COM_y	-10.3	-10.3	-4.9	-2.4	4.3	mm
COM_z	21.	21.	11.5	12.9	-36.2	mm

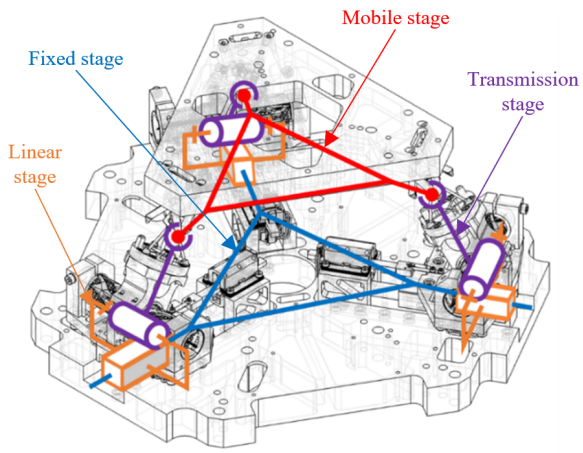

Figure 4. Diagram of the mirror positioning mechanism.

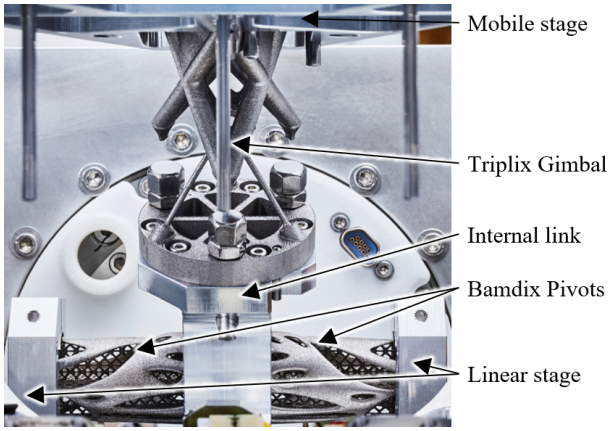

Figure 5. Flexible transmission stage of an active SMT.

design and assembly, but increases the complexity of the mechanism calibration. In this configuration, the use of flexure-based joints in the transmission stage is essential to avoid backlash and hysteresis effects.

The flexible transmission stage links the actuated radial carriage to the mobile platform of the SMT. As illustrated in Fig. 5, it is composed of two pivot supports, two flexure pivots named Bamdix, one internal link, and one flexure gimbal named Triplix. Both Triplix and Bamdix joints are printed in stainless steel 17-4PH (Young modulus of 193 GPa) through Laser Powder Bed Fusion (LPBF). This is done to demonstrate the capabilities of this advanced manufacturing method for high precision mechanism applications.

To reach the targeted accuracy, the two mechanisms underwent multiple calibration sequences. First, each linear stage is individually calibrated to compensate for intrinsic errors and encoder misalignment. This procedure allows the linear stage to be positioned over its full 20 mm range of motion with an accuracy better than ±2 µm and a resolution better than 350 nm. Then, each of the mirror tile positioning mechanisms is fully calibrated using a three-axis

Table 2. Mirror positioning mechanism performances.

		SMT 4	SMT 5	
Accuracy	θ_x	88.0	99.0	µrad
	θ_y	86.8	100.4	µrad
	z	5.5	6.2	µm
Repeatability	θ_x	6 ± 1.5	8.0 ± 3.9	µrad
	θ_y	3.7 ± 1.3	3.7 ± 1.2	µrad
	z	0.6 ± 0.2	0.3 ± 0.2	µm

interferometer and an autocollimator, precisely measuring the mirror platform position across 8000 mirror postures. From these measurements, a calibrated Inverse Geometric Model (IGM) is calculated using a cubic order polynomial model determined with the use of a step-wise regression algorithm. This model connects the mirror posture coordinates to the three actuators linear coordinates. The calibrated model is then implemented in the mirror tile control software. Results obtained after calibration of both active SMTs are presented in Table 2. Here, the accuracy is the standard deviation of the measured errors obtained over 512 verification points (that were not used for calibration). Repeatability values are computed by reaching 64 positions for SMT4 and 91 for SMT5, 10 times each. The order in which these positions are reached has been randomized so that no bias is expected. Additional details regarding the design, calibration and performance of the SMTs are provided in [20].

Hotdock standard interconnect

The connection between the mirror tiles is achieved using standard interconnects that guarantee mechanical, data, power and thermal connectivity between components. The interfaces selected for the project are called HOTDOCKs [19], and they are used to fix the SMTs in the assembly area and to manipulate the SMTs with the robotic system during the assembly process. Fig. 6 represents the intended assembly, with six mirror tiles, and multiple HOTDOCK connectors between them. It also shows the HOTDOCK interconnect, a small cylinder with four protrusions (petals) on its upper side that guide the connection between two interfaces, thus reducing the influence of positional and rotational uncertainties during the latching process. The HOTDOCKs have a compact and fully-integrated androgynous and 90-degree symmetrical design. The central connection plate is equipped with spring-loaded POGO pin connectors, which offers re-configurable and switchable electrical power as well as bi-directional high rate data transfer between connected subsystems. There are basically two versions of the interconnect: an active one, which provides an actuation mechanism for the coupling as well as integrated control and interface electronics, and a passive one without active components. Both Active-to-Active and Active-to-Passive connections are possible, although for this demonstration we relied only on Active-to-Passive connections. The control interface of the active version provides feedback about all process states so that execution can be monitored in all phases. The successful latching of individual connections and the overall structural integrity can thus be verified.

Robotic assembly system

The platform performing the assembly demonstration is based on a KUKA KMR iiwa robot (Fig. 7). It consists of a manipulator mounted on a mobile base with omnidirectional wheels, providing planar navigation (3 degrees of freedom) based on a laser scanner. The robotic manipulator is a

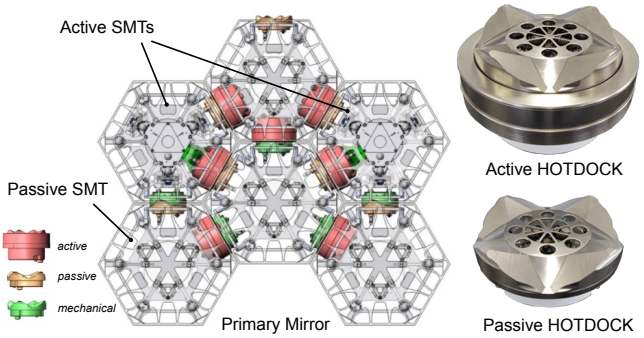

Figure 6. Configuration of active, passive and mechanical HOTDOCKs for the dPAMT scenario.

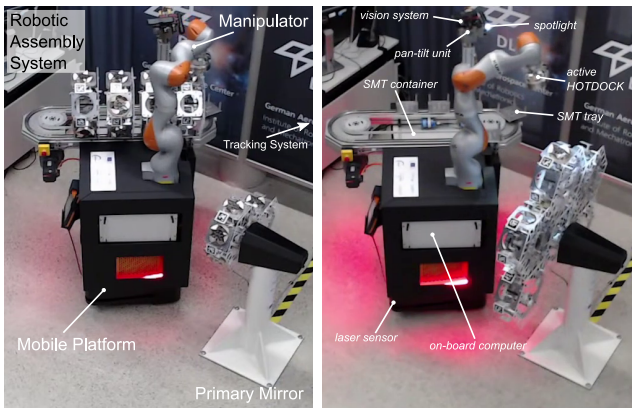

Figure 7. Overview of major components of the robotic assembly system based on a KUKA KMR mobile robotic platform.

KUKA LBR iiwa 14 R820, a compliant arm with 7 degrees of freedom and torque sensors at each joint, which allows operation in both position and torque control modes. The arm has a nominal payload up to 14 kg and maximum reachability of 820 mm. Next to the arm, an SMT container is mounted. The container is a carousel that moves the SMTs to a pickup location. The SMTs are graspable with the active HOTDOCK interface, which is mounted at the flange of the robotic arm via an adapter. Additionally, the platform provides a custom pan/tilt camera unit mounted on a pole for enabling vision-based applications.

Assembly planning

The assembly planning problem is solved using a Hybrid Planner, consisting of a logical (high-level) and a physical (low-level) planning layers. The planner is capable of computing assembly sequences considering a diverse set of semantic, structural, and physical constraints. It verifies that the overall design and its intermediate states are feasible with respect to signal and load transfer, and guarantees structural stability of each assembly substep. Additionally, it is capable of selecting the path that minimizes a desired total cost considering multiple constraints.

The assembly is represented as a graph, as shown in Fig 8. In this representation, nodes are mapped to partial assemblies of the telescope, while the edges indicate the transitions

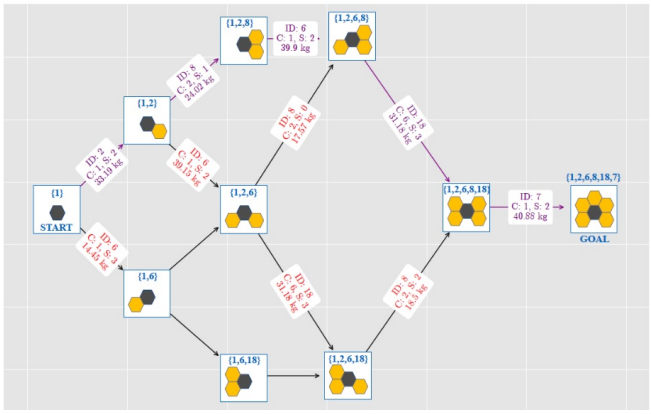

Figure 8. Graph generated by the Hybrid Planner for the dPAMT scenario. Each node represents intermediate states of the assembly process. The edges contain information about the maximum weight the tile to be placed can have.

between nodes. Every edge contains the information about the maximum weight that the next tile can have in order to be compliant with the physical restrictions of the robotic system. The values included in the edges are computed in the physical layer, meanwhile the search for the optimal sequence of tasks is done in the logical layer.

The hybrid planner successfully finds a path (sequence) from the initial state to the complete assembly, maximizing the allowed mirror tile weight for such assembly sequence (which provides an indication of the safety margin considering the robot load). At the local level, smooth collision-free trajectories are obtained, which are far from the maximum operating limits of the joints. Also, the path minimizes a desired cost function, in this particular case the joint torques, allowing the robot to execute the trajectories safely even when carrying heavy payloads. This minimization of the cost function is achieved by the implementation of the Stochastic Trajectory Optimization for Motion Planning (STOMP) [21]. At the high-level layer, the search of an assembly sequence is performed on a multigraph. To find the best path, a MiniMax Cost Search is implemented. The hybrid planner has not only succeeded in maximizing the mirror tile weight the robotic arm can lift, but it can also be used to minimize inertial changes in the assembly states, facilitating the assembly process in an on-orbit scenario. Details regarding the assembly planner are provided in [22].

Skill engine and robot control

The generated assembly sequence represents high level tasks on a logic level and can be further decomposed into subtasks. For instance, the assembly of a SMT requires first to move the next SMT in the carousel to the pickup location, then to pick up the SMT from the carousel, and finally to join it with the SMTs on the already finished parts of the mirror. All these subtasks can be carried out by the robotic system using its skill set, which encapsulates the robot capabilities in a configurable and reusable way.

Skills can be adapted to the current task, and the desired behavior can be guaranteed to solve a class of tasks through a certification process. The parameters for a specific skill are set based on the geometric and environmental conditions of the robot at the time of ex-

ecution. The major skills implemented in the system are: `move_mobile_base`, `pick_smt`, `place_smt`, `verify_assembly`, and `move_smt_to_pickup`, which is used to control the SMT trays in the carousel. Each skill has a set of parameters which allows to apply them in all occurring situations in the given scenario. Internally, these skills call further lower-level system functions, such as the function to localize the mobile base with respect to the assembly area, the functions to latch and unlatch the HOTDOCK connections, and the commands for the robotic manipulator control.

To ensure compliant interactions of the arm while performing the assembly steps, and to cope with geometric uncertainty in the environment, we rely on Cartesian impedance control. In particular, this control mode is used during the coupling of two interfaces at the pick-up of a SMT from the container, and during the assembly of a SMT to the mirror with at least a single- and up to a triple HOTDOCK connection. The default Cartesian impedance controller of the KUKA RoboticsAPI is used in all situations in which contact interaction occurs, whereas the position controller is employed during the contact-free transfer motions, as the execution with the position controller can be considered to be more accurate with respect to path deviations. The execution of paths with the impedance controller is typically more strongly affected by dynamical effects. Therefore, the position controller is more suitable for the execution of the paths generated by the motion planner to avoid collisions. Controller switches from position control to impedance control can be triggered in real time at the event of sensed contacts. The combination of both controller modes enables a robust implementation of assembly skills that can deal with geometric uncertainties in the poses of the SMTs.

In our system, two basic compliant control strategies are investigated, as visualized in Fig. 9. Strategy A is suitable for small geometric uncertainties and largely benefits from the geometrical guidance properties of the HOTDOCK form-fits. Strategy B is suitable for larger geometric uncertainties as it includes an additional oscillating force/torque-overlay in the task space. In this way, a blind search strategy can be implemented, which is more robust but also less time efficient.

The compliance frame for the Cartesian impedance controller is located at the center of the planar face of the HOTDOCK for the single connection, and the approach direction of the contact motion is along the direction normal to the face. For the double connection, the compliance frame and the approach motion are located at half the angle between the two interfaces. In the case of simultaneous connection of three interfaces, the central one is chosen for the compliance and for defining the principal motion direction of the assembly strategy. The system can compute from its internal world model which case applies, and plans the motion accordingly. In all cases, the lateral stiffness of the controller is reduced to allow the uncertainty compensation motion according to the chosen strategy and benefit from the form fit geometry of the interface.

The assembly skills are implemented using the KUKA RoboticsAPI in Java, and are made available to the execution flow control system via the DLR middleware Links_and_nodes. The output of the assembly planner is automatically mapped to the required skills of the robotic system. Based on this mapping given as an XML document, a state machine is automatically generated, which can be

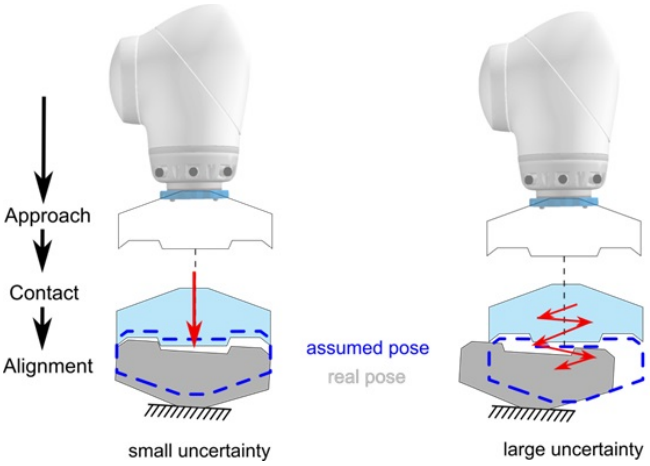

Figure 9. Compliant control strategies. Strategy A (left) is designed for small uncertainty in the assumed pose; Strategy B (right) for larger uncertainty.

used for the execution of the assembly process using the DLR RAFCON software[1]. RAFCON provides a graphical user interface for the state machine and allows implementing hierarchically-structured programs composed of robotic skills [23].

Visual perception

Visual perception is crucial for enabling full autonomous robotic applications. For assembly process monitoring, we rely on fiducial markers detection to compute the tile pose and detect potential misalignments (Fig. 10). With a calibrated camera mounted on the robotic platform, vision is triggered by the high-level skill engine to provide the 3D pose of the object of interest.

Estimating the camera intrinsic parameters (i.e. focal lengths, principal point coordinates, distortion parameters) can be achieved through a classical camera calibration procedure [24]. Pose of the object of interest can then be computed by solving the Perspective-*n*-Point (P*n*P) problem [25], using known 3D object point coordinates and corresponding extracted 2D image point coordinates from fiducial markers detection. To estimate the pose of the camera with respect to the robotic arm coordinate system, a hand-eye calibration procedure [26] is performed to obtain the transformation between the camera frame and the robot end-effector/tool center point (TCP) frame.

Motivations about using the AprilTag-3 [27] visual markers in this application are multiple. Its permissive license (BSD 2-Clause License) and full source code availability[2] allow easy integration into the codebase. It provides accurate marker corners extraction [28][29], which is essential for robust pose computation. Drawbacks of AprilTag-3 visual markers are more expensive computation time compared to its principal alternative (ArUco, [30]), and its inability to detect partially occluded markers. These disadvantages are non-blocking in our use case and counterbalanced by its localization accuracy and its wide use in robotic applications.

[1]RAFCON is an open source (EPL) software available at `https://dlr-rm.github.io/RAFCON/`
[2]`https://github.com/AprilRobotics/apriltag`

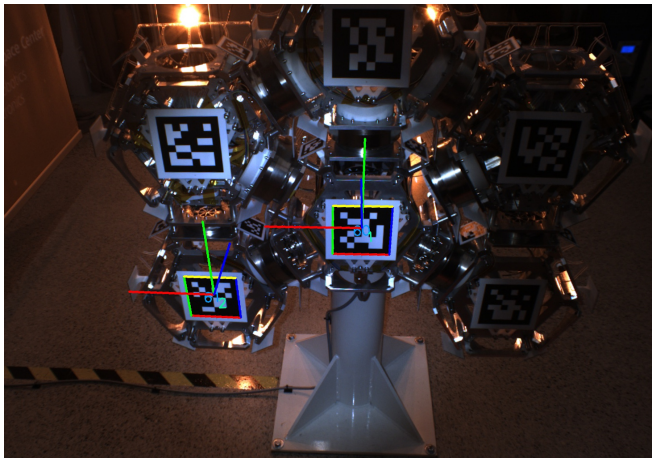

Figure 10. Detected AprilTag markers and computed SMT poses from visual perception.

On each SMT, small AprilTag markers (65 x 65 mm) are precisely positioned beside each HOTDOCK, and one big marker (150 x 150 mm) is positioned at the back of the mirror tile. This should ensure correct SMT localization for various viewpoints. AprilTags detection and pose estimation for assembly area localization using the big markers provides a reliable detection and precise results at working distances between 1 m and 3 m given a focal length of 6 mm with a 1/1.8" sensor of 1624 x 1234 pixels resolution; the small markers are suitable for distances between 0.1 m and 0.75 m and appropriate for SMT localization during grasping and assembly monitoring. AprilTag 36h11 family is used since this family provides robust tag decoding and 587 unique tag ids (each marker must be unique for our use case). There is indeed a trade-off between the number of tag ids in a family and the robustness involved during the tag id decoding process. The model of the AprilTag markers is computed from the tile CAD model.

On Fig. 10, detected markers are highlighted and the computed poses of the SMTs are visualized using overlayed coordinates frames in the image. The tile id is also displayed, and the assembly process monitoring can be performed by computing the relative pose between two tiles and verifying that the pose error does not exceed some acceptable value.

4. Experimental Results

Assembly strategy evaluation

First, the assembly strategies for the connection of the interfaces of the SMTs were investigated to find appropriate parameters for enabling a robust assembly. The robustness against pose uncertainty can be analysed by using the concept of regions of attractions (ROA) [31]. These regions depend on the geometry of the contact areas and describe the relative configuration space between the objects in which a convergence to the goal configuration is possible by applying the motion strategy. This can be a pushing motion in a certain direction, or as in our case, the Strategy A and B as described in Section 3. An analysis was carried out during the preliminary design phase to investigate single, double and triple HOTDOCK connections using a mock-up (Fig. 11). For the evaluation, the assumed pose of the object is varied

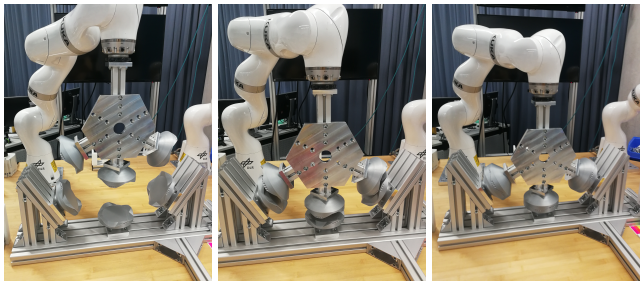

Figure 11. Mock-up to investigate the robustness of the assembly strategies.

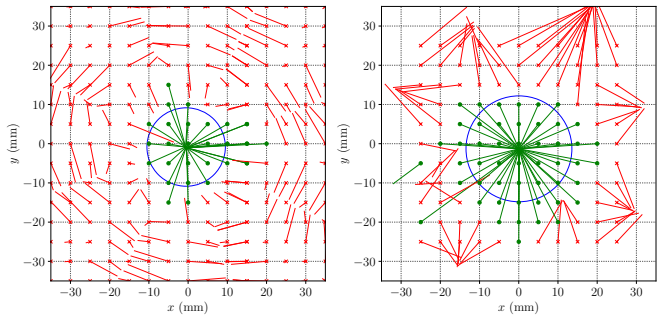

(a) Strategy A (b) Strategy B

Figure 12. Region of attraction (ROA) of a single connection under the presence of an position uncertainty in the $xy-$plane of the contact surface. Offsets of $5\,\mathrm{mm}$ were systematically investigated in a mock-up with printed interfaces for the two strategies. The plots show the start and the reached pose projected into the $xy-$plane connected with a line. Successful runs (green) reach the center, while runs starting outside of the ROA (approximated with a blue circle) fail (red).

systematically and parameters of the controllers are tuned to have a large region. Fig. 12 shows the regions for a single connection and a position uncertainty in the $xy-$plane of the contact surface. It can be seen that strategy B is more robust than strategy A and allows offsets up to $15\,\mathrm{mm}$ of misalignment. Based on the insights obtained from the mock-up, strategy B was chosen for the demonstration using the actual hardware and tuned such that it shows reliable behavior in all considered cases. Note in this context that the same stiffness parameters are used independently of the number of connections, and only the location of the compliance frame is adapted, as described in Section 3. This has shown to be sufficiently robust also in the cases of up to three connections. However, an increase of the performance could potentially be achieved by an optimization of the compliance parameters for each individual case.

The different phases of the finally implemented strategy are visible in the force and torque profile over time. Fig. 13 shows the data obtained from joint torque measurements during the execution of a `pick_smt` skill. In the beginning, the position controller is used to achieve the most accurate approach as possible. Once the contact is detected by the peak of the force measurement, the controller switches to

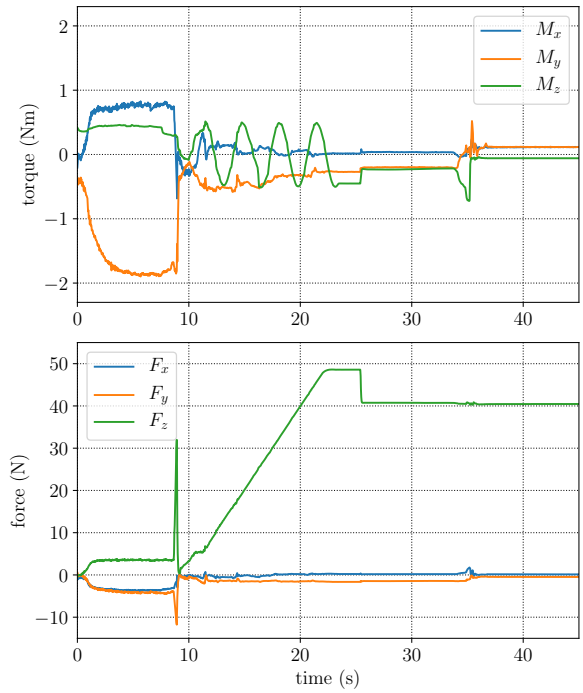

Figure 13. Force and torque at the HOTDOCK reference frame estimated from the joint torque measurements during the execution of the `pick_smt` skill. At time $\approx 9\,\mathrm{s}$ contact is detected and the switch to the impedance controller is triggered, which uses an oscillation with an amplitude of $0.5\,\mathrm{N\,m}$ in M_z to support the rotational alignment. The normal force F_z increases linearly according to the configured Cartesian stiffness. After the alignment has finished ($\approx 25\,\mathrm{s}$) the controller presses with a constant force of $40\,\mathrm{N}$ to keep a stable contact during the latching of the HOTDOCK. At time $\approx 35\,\mathrm{s}$ the mechanical latching process has finished.

compliant impedance controller. During the alignment phase, the oscillation around the normal direction can be seen in the measurement of the torque M_z which makes it very robust against the orientation uncertainty in combination with the Cartesian impedance to compensate position uncertainty.

Autonomous assembly

The assembly planning framework described in Section 3 is used to generate an appropriate sequence of assembly tasks offline and map them to robotic skills. Listing 1 shows an excerpt of a generated XML file for the assembly of the first SMT. The parameters of the skills are used to retrieve further information about the associated object instances inside the skill implementation, e.g. load data of the SMT or the relative transformation for a particular grasping angle. Here, each SMT and each HOTDOCK have a unique identifier, SmtUid and HotdockUid, respectively. Furthermore, all relative transformations between the objects are referenced semantically using labeled places at the objects, e.g. PlaceHotdockId and PlaceSmtId. The physical quantities associated with the labels are then obtained from the internal world model and from sensory input. In this way, the skill execution can be easily adapted to all tasks to be solved during the assembly. At the execution stage, the robotic assembly system is fully autonomous using its sensor systems to navigate and localize the assembly area. The full sequence of assembly is depicted in Fig.14, a video is available online [32]. It contains in total 18 skills and requires $\approx 32\,\mathrm{min}$ to assemble the 5 SMTs of the demonstrator. At the end of the assembly, the final poses of the mirror tiles are verified using the AprilTag markers. The visual reconstruction allows to detect correct and false alignments at a coarse level. This was tested for multiple scenarios (see Fig. 15).

Listing 1. XML specification of the first assembly task in the full sequence of the assembly.

.

```
<Task smtID="2" id="1" name="place_smt_task">
  <Sequence>
    <Skill type="move_smt_to_pickup" id="5" name="skill_5">
      <SmtUid>2</SmtUid>
    </Skill>
    <Skill type="pick_smt" id="6" name="skill_6">
      <SmtUid>2</SmtUid>
      <PlaceHotdockId>1</PlaceHotdockId>
      <Grasp>270</Grasp>
      <HotdockUid>HD-PUL-028-P</HotdockUid>
      <JointPath>1_SMT_2/0_move_to_app_pose.csv</JointPath>
      <Velocity>0.2</Velocity>
    </Skill>
    <Skill type="place_smt" id="7" name="skill_7">
      <SmtUid>2</SmtUid>
      <PlaceHotdockId>1</PlaceHotdockId>
      <Grasp>270</Grasp>
      <PlaceSmtId>6</PlaceSmtId>
      <HotdockUid>HD-PUL-028-P</HotdockUid>
      <JointPath>1_SMT_2/3_move_to_assembly_app.csv</JointPath>
      <Velocity>0.2</Velocity>
    </Skill>
  </Sequence>
</Task>
```

Assembly evaluation

In order to measure how the autonomous robotic system impacts the assembly of the telescope, the following experiment was carried out. First, the primary mirror is manually assembled. An expert places the mirror tiles manually and then commands the respective HOTDOCKs to latch. This process is repeated for each individual tile. Once the assembly is completed, the relative position of the mirror tiles are measured with the VICON system to obtain a ground truth measurement. Then, the complete assembly is performed autonomously by the robotic system. The expert only initiates the assembly by the start command and does not have any other intervention during the whole process. After the assembly is completed, the relative pose of the mirror tiles is measured with the VICON system. The experiment was repeated 10 times for each modality of assembly (manual and autonomous).

Fig. 16 shows the result for both cases. All measurements were taken relative to the central tile, with a reference coordinate system at its center. The robotic assembly system achieves a precise assembly with a remaining error of up to $\approx 2.5\,\mathrm{mm}$ in position and $\approx 0.35°$ in orientation. In an additional accuracy analysis, we compare the averaged displacements achieved by the robotic execution with the average over all human runs, which is considered to be the best achievable result given gravitational effects and deformations of the structure. The pose errors with respect to the average of the manual assembly are summarized in Table 3. The accuracy in position is below $1\,\mathrm{mm}$ and for orientation below $0.2°$.

In conclusion, the achieved precision in the autonomous execution is sufficient for a successful assembly and stable connection between the SMTs. The remaining error

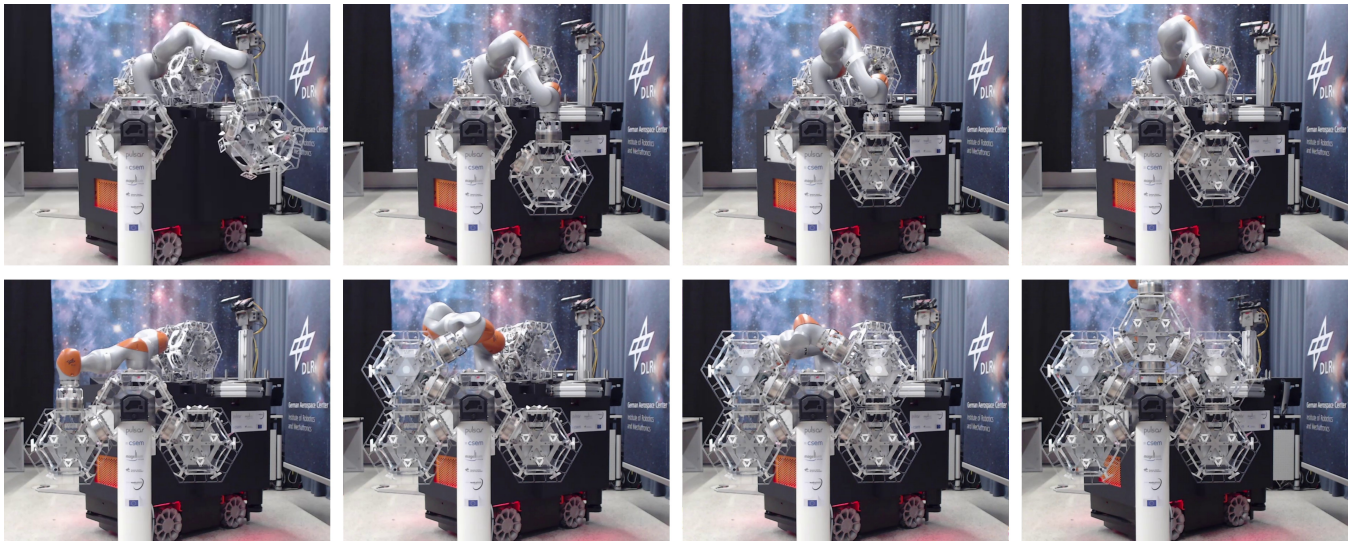

Figure 14. Full sequence of assembly. The first row shows the approach and placement of the SMT 2 with a single HOTDOCK connection. The second row shows the assembly of SMT 3 (single connection), SMT 4-5 (dual HOTDOCK connection), and SMT 6 (triple HOTDOCK connection).

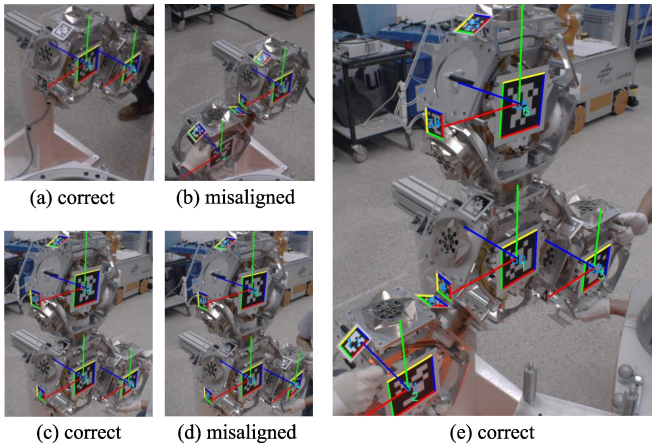

Figure 15. Examples for the visual reconstruction of the assembly using the fiducial markers, and qualitative verification of the alignment.

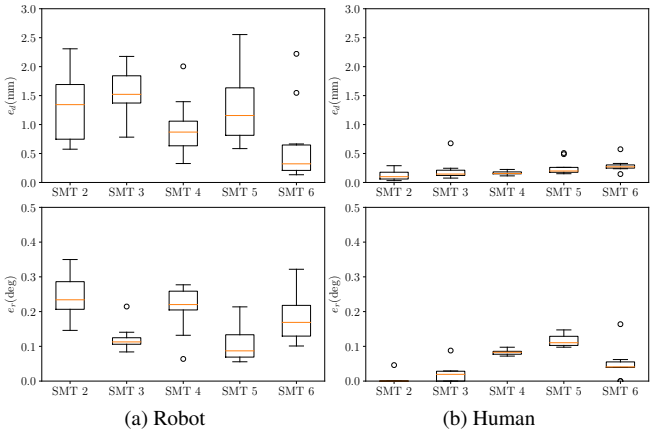

Figure 16. Precision of the final assembly for the autonomous (a) and manual (b) assembly execution. The boxplots in the upper row show the error distributions of the distance e_d between the reached position of the center of the SMT and the average position over all runs; below the distribution of the error in the orientation e_r.

can be compensated with the mirror positioning mechanism (Section 3) as was tested by focusing the mirrors of the active SMTs on a common reference point. However, a gap remains in comparison with the human precision. In the current implementation, additional localization methods were not considered, in order to keep the system complexity small. During the final phase of the assembly process no active localization is executed, the impedance control strategy ensures a reliable alignment. Improvements could potentially be achieved by the integration of more accurate sensor-based localization methods using the tactile sensory information or high precision optical measurements. This fusion of multiple sensory inputs at a high rate is naturally achieved by humans, giving them the advantage in these kind of tasks. Furthermore, the assembly strategy including the choice of the compliance and motion directions is currently implemented in a basic form that supports all cases sufficiently, but which could be improved to get better performance. For example, in the case of multiple connections, the compliance frame and the related control force could be changed during the process such that it always guarantees good alignment for the pair of HOTDOCKs to be latched. Also, more advanced assembly strategies could be learned in dedicated training environments using reinforcement learning or similar approaches.

5. Conclusion

This paper presented a demonstrator for assembling segmented mirror tiles using a mobile robotic assembly system, testing aspects such as autonomous assembly and optical

Table 3. Accuracy of the final pose of the SMTs assembled by the robot measured with respect to the human reference assembly. 10 runs were executed by the robot as well as by the human to compute the average values.

SMT	2	3	4	5	6	
pos.	0.969	0.977	0.358	0.691	0.392	mm
ori.	0.151	0.081	0.129	0.110	0.070	deg

verification of the assembled mirror. It proved the feasibility of autonomous assembly of the primary mirror, using a combination of adaptable perception, integrated assembly and motion planning, and compliant control of the manipulators. HOTDOCK was effectively employed as standard interconnect, and enabled the assembly and manipulation of multiple components. The SMTs provided a modular approach for constructing a large mirror, facilitating the manipulation and providing high motion accuracy and adjustment of the optical surfaces, as required for a space telescope. The knowledge gained in this demonstrator has strong synergies with other ground-based applications, where collaborative robots are used for assembling different structures, for instance, using modular construction kits [33].

The next step is to prove the feasibility of orbital assembly in a suitable mission. This will definitely show the ability of autonomous robotics to perform complex orbital tasks, as required for future constructions of large structures directly in space.

ACKNOWLEDGMENT

This project has received funding from the European Union's Horizon 2020 research and innovation programme under grant agreement No 821858, project PULSAR.

REFERENCES

[1] J. Gardner, J. Mather, M. Clampin, R. Doyon, M. Greenhouse, H. Hammel, J. Hutchings, P. Jakobsen, S. Lilly, K. Long, J. Lunine, M. McCaughrean, M. Mountain, J. Nella, G. Rieke, M. Rieke, H. Rix, E. Smith, G. Sonneborn, M. Stiavelli, H. Stockman, R. Windhorst, and G. Wright, "The James Webb Space Telescope," *Space Science Reviews*, vol. 123, no. 4, pp. 485–606, 2006.

[2] M. A. Roa, K. Nottensteiner, G. Grunwald, S. Andiappane, M. Rognant, A. Verghaege, and V. Bissonnette, "In-space robotic assembly of large telescopes," in *Proc. Symp. on Advanced Space Technologies in Robotics and Automation - ASTRA*, 2019.

[3] M. Rognant, C. Cumer, J.-M. Biannic, M. A. Roa, A. Verhaeghe, and V. Bissonnette, "Autonomous assembly of large structures in space: a technology review," in *Proc. Europ. Conf. for Aeronautics and Aerospace Sciences (EUCASS)*, 2019.

[4] P. Letier, X. Yan, M. Deremetz, A. Bianco, G. Grunwald, M. Roa, M. Krenn, M. Munoz, P. Dissaux, J. Garcia, R. Ruiz, L. Filippis, G. Porceluzzi, M. Post, M. Walshe, and P. Perryman, "MOSAR: MOdular Spacecraft Assembly and Reconfiguration demonstrator," in *Proc. Symp. on Advanced Space Technologies in Robotics and Automation - ASTRA*, 2019.

[5] M. A. Roa, C. Koch, M. Rognant, A. Ummel, P. Letier, A. Turetta, P. Lopez, S. Trinh, I. Rodriguez, K. Nottensteiner, J. Rouvinet, V. Bissonnette, G. Grunwald, and T. Germa, "PULSAR: Testing the technologies for on-orbit assembly of a large telescope," in *Proc. Symp. on Advanced Space Technologies in Robotics and Automation - ASTRA*, 2022.

[6] N. Inaba and M. Oda, "Autonomous satellite capture by a space robot: world first on-orbit experiment on a japanese robot satellite ETS-VII," in *Proc. IEEE Int. Conf. Robotics and Automation - ICRA*, 2000, pp. 1169–1174.

[7] G. Visentin and F. Didot, "Testing space robotics on the japanese ets-vii satellite," *ESA bulletin*, vol. 99, pp. 61–65, 1999.

[8] B. Ma, Z. Jiang, Y. Liu, and Z. Xie, "Advances in space robots for on-orbit servicing: A comprehensive review," *Advanced Intelligent Systems*, p. 2200397, 2023.

[9] M. A. Roa, K. Nottensteiner, A. Wedler, and G. Grunwald, "Robotic Technologies for In-Space Assembly Operations," in *Proc. Symp. on Advanced Space Technologies in Robotics and Automation - ASTRA*, 2017.

[10] E. Papadopoulos, F. Aghili, O. Ma, and R. Lampariello, "Robotic manipulation and capture in space: A survey," *Frontiers in Robotics and AI*, p. 228, 2021.

[11] B. Karlow, C. Jewison, D. Sternberg, S. Hall, and A. Golkar, "Tradespace investigation of strategic design factors for large space telescopes," *J. of Astronomical Telescopes, Instruments, and Systems*, vol. 1, no. 2, p. 027003, 2015.

[12] G. Cataldo, M. Chodas, P. Davé, A. Dixit, S. Hall, D. Hayhurst, F. Hicks, C. Jewison, I. Josan, B. Karlow, B. Mccarthy, A. Owens, E. Peters, M. Shaw, D. Sternberg, K. Voelbel, and M. Wu, "Tradespace Investigation of a Telescope Architecture for Next-generation Space Astronomy and Exploration," MIT Department of Aeronautics and Astronautics, Tech. Rep., 2014.

[13] H. Thronson, M. Bolcar, M. Clampin, J. Crooke, L. Feinberg, W. Oegerle, N. Rioux, P. Stahl, and K. Stapelfeldt, "Path to a UV/optical/IR flagship: review of ATLAST and its predecessors," *J. of Astronomical Telescopes, Instruments, and Systems*, vol. 2, no. 4, p. 041210, 2016.

[14] M. Bolcar, S. Aloezos, V. Bly, C. Collins, J. Crooke, C. Dressing, L. Fantano, L. Feinberg, K. France, G. Gochar, Q. Gong, J. Hylan, A. Jones, I. Linares, M. Postman, L. Pueyo, A. Roberge, L. Sacks, S. Tompkins, and G. West, "The large UV/Optical/Infrared surveyor (LUVOIR): Decadal mission concept design update," in *Proc. SPIE UV/Optical/IR Space Telescopes and Instruments: Innovative Technologies and Concepts*, 2017.

[15] C. Saunders, D. Lobb, M. Sweeting, and Y. Gao, "Building large telescopes in orbit using small satellites," in *Proc. Int. Astronautical Congress (IAC)*, 2016.

[16] S. Basu, T. Mast, and G. Miyata, "A proposed autonomously assembled space telescope (AAST)," in *AIAA Space Conf.*, 2003.

[17] R. Polidan, J. Breckinridge, C. Lillie, H. MacEwend, M. Flannerya, and D. Dailey, "An evolvable space telescope for future UV/Opt/IR astronomical missions,"

in *Proc. SPIE, Space Telescopes and Instrumentation: Optical, Infrared, and Millimeter Wave*, 2015.

[18] N. Lee, P. Backes, J. Burdick, S. Pellegrino, C. Fuller, K. Hogstrom, B. Kennedy, J. Kim, R. Mukherjee, C. Seubert, and Y. Wu, "Architecture for in-space robotic assembly of a modular space telescope," *J. of Astronomical Telescopes, Instruments, and Systems*, vol. 2, no. 4, p. 041207, 2016.

[19] P. Letier, T. Siedel, M. Deremetz, E. Pavlovskis, B. Lietaer, K. Nottensteiner, M. Roa, J. Sanchez, J. Corella, and J. Gancet, "HOTDOCK: Design and Validation of a New Generation of Standard Robotic Interface for On-Orbit Servicing," in *Proc. Int. Astronautical Congress (IAC)*, 2020.

[20] J. Rouvinet, A. Ummel, F. Cosandier, D. Nguyen, and V. Schaffter, "PULSAR: Development of a mirror tile prototype for future large telescopes robotically assembled in space," in *Proc. SPIE Conf. on Astronomical Telescopes + Instrumentation*, 2020.

[21] M. Kalakrishnan, S. Chitta, E. Theodorou, P. Pastor, and S. Schaal, "STOMP: Stochastic trajectory optimization for motion planning," in *Proc. IEEE Int. Conf. Robotics and Automation (ICRA)*, 2011, pp. 4569–4574.

[22] J. Martinez, I. Rodriguez, K. Nottensteiner, J. P. Lutze, P. Lehner, and M. A. Roa, "Hybrid Planning System for In-Space Robotic Assembly of Telescopes using Segmented Mirror Tiles," in *Proc. IEEE Int. Conf. Aerospace - AEROCONF*, 2021.

[23] S. G. Brunner, F. Steinmetz, R. Belder, and A. Dömel, "Rafcon: A graphical tool for engineering complex, robotic tasks," in *Proc. IEEE/RSJ Int. Conf. on Intelligent Robots and Systems - IROS*, 2016, pp. 3283–3290.

[24] Z. Zhang, "A flexible new technique for camera calibration," *IEEE Trans. on Pattern Analysis and Machine Intelligence*, vol. 22, pp. 1330–1334, 2000.

[25] E. Marchand, H. Uchiyama, and F. Spindler, "Pose Estimation for Augmented Reality: A Hands-On Survey," *IEEE Trans. on Visualization and Computer Graphics*, vol. 22, no. 12, pp. 2633 – 2651, 2016.

[26] R. Y. Tsai and R. K. Lenz, "A new technique for fully autonomous and efficient 3D robotics hand/eye calibration," *IEEE Trans. on Robotics and Automation*, vol. 5, pp. 345–358, 1989.

[27] M. Krogius, A. Haggenmiller, and E. Olson, "Flexible layouts for fiducial tags," in *Proc. IEEE/RSJ Int. Conf. on Intelligent Robots and Systems - IROS*, 2019, pp. 1898–1903.

[28] J. Kallwies, B. Forkel, and H.-J. Wuensche, "Determining and Improving the Localization Accuracy of AprilTag Detection," in *Proc. IEEE Int. Conf. Robotics and Automation - ICRA*, 2020, pp. 8288–8294.

[29] G. Yu, Y. Hu, and J. Dai, "TopoTag: A Robust and Scalable Topological Fiducial Marker System," *IEEE Trans. on Visualization and Computer Graphics*, vol. 27, no. 9, pp. 3769–3780, 2021.

[30] F. Romero-Ramirez, R. Muñoz-Salinas, and R. Medina-Carnicer, "Speeded up detection of squared fiducial markers," *Image and Vision Computing*, vol. 76, pp. 38–47, 2018.

[31] A. Stemmer, A. Albu-Schaffer, and G. Hirzinger, "An analytical method for the planning of robust assembly tasks of complex shaped planar parts," in *Proc. IEEE Int. Conf. Robotics and Automation - ICRA*, 2007, pp. 317–323.

[32] K. Nottensteiner, I. Rodríguez, and M. A. Roa, "Demonstration of the Autonomous Precise Assembly of Segmented Mirror Tiles for a Space Telescope," Oct. 2023. [Online]. Available: https://doi.org/10.5281/zenodo.8413958

[33] I. Rodriguez, K. Nottensteiner, D. Leidner, M. Durner, F. Stulp, and A. Albu-Schaffer, "Pattern recognition for knowledge transfer in robotic assembly sequence planning," *IEEE Robotics and Automation Letters*, p. 3666–3673, 2020.

BIOGRAPHY

Máximo A. Roa is a Senior Scientific Researcher and Group Leader for "Robotic Planning and Manipulation" at the Institute of Robotics and Mechatronics, German Aerospace Center (DLR).

Korbinian Nottensteiner is a Team Leader and Scientific Researcher at the Institute of Robotics and Mechatronics, German Aerospace Center (DLR).

Ismael Rodríguez is a Scientific Researcher at the Institute of Robotics and Mechatronics, German Aerospace Center (DLR).

Timo Bachmann is a Scientific Researcher at the Institute of Robotics and Mechatronics, German Aerospace Center (DLR).

Jean-Pascal Lutze is a Scientific Researcher at the Institute of Robotics and Mechatronics, German Aerospace Center (DLR).

Pierre Letier is a Project Manager at Space Application Services, Belgium.

Antoine Ummel is a Project Manager in "System Engineering for Space Applications" at CSEM, Switzerland.

Julien Rouvinet is a Senior R&D Engineer at CSEM, Switzerland.

Florent Cosandier is an R&D Expert at CSEM, Switzerland.

David Nguyen is an R&D Engineer at CSEM, Switzerland.

Virginien Schaffter is a Senior R&D Engineer at CSEM, Switzerland.

Souriya Trinh is a Research Engineer at Magellium, France.

Vincent Bissonnette is a Research Engineer at Magellium, France.

Thierry Germa is a Project manager at Magellium, France.